THE JOURNAL OF PHYSICAL CHEMISTRY C

Article

pubs.acs.org/JPCC

Effect of Nanocrystalline Domains in Photovoltaic Devices with Benzodithiophene-Based Donor–Acceptor Copolymers

Christopher Menelaou,[†] Steve Tierney,[‡] Nicolas Blouin,[‡] William Mitchell,[‡] Priti Tiwana,[‡] Ian McKerracher,[§] Chennupati Jagadish,[§] Miguel Carrasco,[‡] and Laura M. Herz*[,†]

[†]Department of Physics, Clarendon Laboratory, University of Oxford, Parks Road, Oxford OX1 3PU, U.K.

[‡]Chilworth Technical Centre, Merck Chemicals Ltd., University Parkway, Southampton SO16 7QD, U.K.

[§]Department of Electronic Materials Engineering, Research School of Physics and Engineering, The Australian National University, Canberra ACT 0200, Australia

Supporting Information

ABSTRACT: We have investigated the effects of thin-film morphology on the photovolatic performance for a series of donor–acceptor copolymers based on benzodithiophene donor and benzothiadiazole acceptor units. Photovoltaic devices incorporating polymer:fullerene blends show highest efficiencies (up to 6%) for those polymers exhibiting the least degree of crystallinity in X-ray diffraction patterns and a corresponding lowest surface roughness in thin films. We find that the existence of such crystalline domains in thin polymer films correlates well with spectral signatures of polymer chain aggregates already present in solution prior to casting of the film. Polymer solubility and casting conditions therefore appear to be crucial factors for enhancing efficiencies of photovoltaic devices based on such donor–acceptor copolymers. To examine why the presence of crystallite domains lowers device efficiencies, we measured exciton diffusion lengths by modeling the time-dependent photoluminescence from thin polymer films deposited on an exciton quencher layer of TiO_2. We find that exciton diffusion lengths in these materials are substantial (4–7.5 nm) and show some variation with polymer crystallinity. However, ultrafast (1 ps) quenching of the polymer emission from polymer:PCBM blends indicates that the vast majority of excitons rapidly reach the charge-dissociating interface, and hence exciton diffusion does not represent a limiting factor. We therefore conclude that the subsequent charge extraction and lifetimes must be adversely affected by the presence of crystalline domains. We suggest that the formed crystallites are too small to offer significant enhancements in long-range charge carrier mobility but instead introduce domain boundaries which impede charge extraction. For this class of materials, polymer designs are therefore required that target high solubility and chain entropy, leading to amorphous film formation.

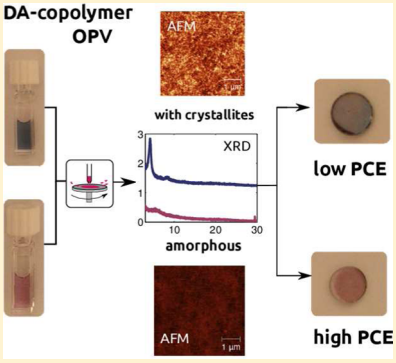

1. INTRODUCTION

Organic photovoltaic devices have high potential as a low-cost, renewable energy source[1,2] and have attracted widespread research interest in recent years, as they are lightweight and flexible and can be processed from solution. Devices typically incorporate mixtures between electron-accepting and -donating materials in order to induce the separation of the initially generated charge-neutral state (molecular exciton) at the interface between the two materials.[3] Since this model was reported, a large number of OPV devices incorporating such type II heterojunction systems have been produced,[3,4] and rapid advances in power conversion efficiencies have been achieved. Devices based on thin films processed directly from solution mixtures (so-called bulk heterojunction films[5]) of π-conjugated polymers and fullerene derivatives now reach power conversion efficiencies of up to 10%.[6] In these polymer:-fullerene systems, high device efficiencies are only obtained after extensive optimization of fabrication conditions, which strongly affect the morphology of the BHJ films.[7] On the one hand, intimate mixing of donor and acceptor materials promotes efficient exciton diffusion to the donor–acceptor interface at which charge transfer can occur. On the other hand, extended crystalline networks are beneficial for efficient charge dissociation[8] and collection.[9] Forming an ideal BHJ requires careful balancing of these processes, and hence small variations in molecular structure, molecular weight, polydispersity, and processing conditions can have significant effects on the overall efficiency.[7,10−12] Such effects have been particularly well documented for the benchmark system of poly(3-hexylthiophene) (P3HT) blended with the fullerene derivative phenyl-C61-butyric-acid-methyl-ester (PCBM), for which high power conversion efficiencies (PCE) of 6%[13,14] have been reached in photovoltaic devices. However, P3HT in many ways represents a highly special case as in its regioregular form it has the strong tendency to form extended crystalline structures of π-stacked polymer chains.[15−17] Such crystalline domains result in a high

Received: April 24, 2014
Revised: July 17, 2014
Published: July 17, 2014

PCE immediately after device fabrication, but extended thermal annealing and/or illumination under full solar conditions (AM1.5) results in phase segregation of the polymer and fullerene components.[18,19] This process can be minimized somewhat by using P3HT with lower regioregularity, which has a lower tendency to crystallize.[20] Likewise, the formation of crystalline PCBM needles on extended thermal annealing causes similar drops in device efficiency which can be mitigated by using modified fullerenes with bulkier substituents than PCBM.[21]

In the quest for higher photovoltaic device efficiencies, donor−acceptor (D−A) copolymers have increasingly been employed as hole transporters.[22−27] Here, the conjugated coupling of electron-donating and -accepting units on the same chain allows a lowering of the band gap energy and therefore an increase in light absorption and photocurrent.[28−30] Several of the recently developed D−A copolymers show that the lessons learnt from the case of P3HT are not necessarily applicable to all polymer:fullerene solar cells. For example, blends of PCDTBT (carbazole/dithienobenzothiadiazole copolymer) and PCBM result in devices with maximum PCE immediatedly after deposition, without any further processing. Any thermal annealing of these devices results in a decrease in chain ordering and a reduction in PCE.[31] Another study demonstrated that in a series of thiophene/quinoxaline copolymers the highest fill factors and PCEs were associated with polymers with the most disordered and twisted backbone that showed the lowest tendency to crystallize.[32] In addition, a fluorinated polymer PBnDT−FTAZ (benzodithiophene/5,6-difluoro-2,1,3-benzothiadiazole copolymer) with low crystallinity was found to yield photovoltaic devices in which the short-circuit current (J_{SC}) and fill factor were insensitive to a doubling of the polymer and fullerene domain sizes.[33] The discrepancy in the trend between device efficiency and crystallinity between P3HT and the more recently developed D−A copolymer materials may be partly understood given that P3HT allows the formation of particularly extended ordered domains or pure polymer when blended with PCBM,[15−17] along with regions of pure PCBM and regions of mixed polymer:PCBM. While large crystallite formation may aid charge mobility in some polymer systems relative to the amorphous polymer phase, the formation of many small ordered regions may prove detrimental because the increasing surface area of the domain boundaries between crystalline and amorphous polymer regions can act as a barrier to charge transfer and promote charge trapping and recombination.[34] Whether device efficiencies increase or decrease with overall film crystallinity should therefore depend on whether the in-domain charge-extraction enhancement or trapping at the domain boundaries is dominant, which in turn is influenced by the crystallite surface-area to volume ratio.

In this study, we examine the interplay between crystallite domain formation and performance in photovoltaic BHJ thin-film devices for a series of donor−acceptor copolymers based on benzodithiophene (BDT) donor and benzothiadiazole (BT) acceptor groups. We examine thin-film morphology and interchain interactions using wide-angle X-ray scattering, atomic force microscopy, and absorption/emission spectroscopy. We find that increased crystallinity of the neat polymer film is associated with lower photovoltaic device efficiencies in BHJ films with $PC_{60}BM$, in agreement with the notion that domain boundaries are impeding performance in this system. We determine the exciton diffusion length in neat films of the polymers by modeling the measured diffusive quenching of excitons at an interface with a compact TiO_2 layer that acts as an electron acceptor. We find that the polymer exhibiting the highest incorporation of crystalline domains exhibits large diffusion lengths of 7.4 nm, while for a polymer film with low crystallinity, a value of only 4.0 nm is extracted. However, measurements of the photoluminescence quenching in polymer:PCBM films indicate that the majority of excitons reach a charge-dissociating interface within about 1 ps after light absorption for all polymers examined. Therefore, exciton diffusion to and dissociation at the BHJ interface does not appear to be a limiting factor in these systems, suggesting that the observed differences in crystallinity predominantly derive from the subsequent steps of charge transport and recombination. We show that for the polymers exhibiting thin films with high crystallinity, chain aggregation is already evident prior to casting, for solution at temperatures below ∼60 °C. For D−A copolymers with moderate to low solubility, casting conditions from solution and the subsequent crystallite formation are hence likely to have a substantial impact on photovoltaic device performance.

2. EXPERIMENTAL METHODS

UV−vis absorbance spectra of polymer films and solutions were measured with a PerkinElmer Lambda 9 UV−vis spectrophotometer. Wide-angle X-ray scattering (WAXS) patterns were taken using a Panalytical X'Pert Pro, with Cu anode ($K\alpha$ = 0.154 nm). Atomic force microscopy (AFM) images were used to assess the surface topography and surface roughness of the polymer films. All measurements were performed with a Veeco Dimension Icon AFM in tapping mode. Photoluminescence (PL) spectroscopy was carried out both in time-resolved and time-integrated (TI) mode. Samples were excited by the frequency-doubled output of a Ti:sapphire oscillator with 80 MHz repetition rate and 100 fs pulse duration. For measurements with subpicosecond (∼350 fs) time resolution, the PL up-conversion (PLUC) method was employed, while time-correlated single photon counting (TCSPC) was used for higher sensitivity, lower resolution measurements. In all experiments, the emitted photoluminescence was collected by a pair of off-axis parabolic mirrors and, in the case of the PLUC experiment, focused onto a β-barium borate (BBO) crystal mounted on a rotation stage to allow tuning of the phase-matching angle. An intense vertically polarized gate beam arriving at the BBO crystal at adjustable time delays was used to up-convert the PL at given times after excitation. The resulting sum-frequency photons were collected, dispersed in a monochromator, and detected by a liquid-nitrogen-cooled CCD. In the TCSPC and TIPL experiments, the BBO crystal was replaced by a Glan-Thompson polarizer to define the detected polarization. For TIPL spectral measurements, photons were detected with a liquid nitrogen cooled CCD and for TCSPC, either by a large-area Hamamatsu PMC-100-20 photomultiplier tube (230 ps instrument response) or a small-area silicon avalanche photodiode (Micro Photon Devices SPD-050-CTE, 35 ps instrument response). For temperature-dependent solution measurements, polymer solutions were held in a quartz cuvette on a home-built temperature controlled stage. For thin-film measurements, samples were held in a dynamic vacuum below 10^{-5} mbar to avoid photodegradation. Excitation pulse fluences of 3, 0.3, and 0.03 μJ cm^{-2} were used for the solid state PLUC, solid state TCSPC, and solution phase TCSPC measurements, respectively. Polymer synthesis

dx.doi.org/10.1021/jp504010x | J. Phys. Chem. C 2014, 118, 17351−17361

was as follows: The electron-donating 4,8-dialkyl-benzodithiophene monomers were prepared by the addition of an alkyl Grignard reagent to 4,8-dialkyl-benzodithiophene-4,8-dione in the case where R_1 = 2-ethylhexyl (i.e., branched alkyl) and in an analogous manner to that reported by Pan et al.[35] in the cases where R_1 = octyl, decyl, dodecyl (i.e., linear alkyl). The electron-accepting 5,6-bis(octyloxy)benzothiadiazole monomer was prepared in an analogous manner to that reported by Bouffard et al.[36] All polymers were prepared by a Stille cross-coupling method in an analgous manner to that reported by Tierney et al.[37] and purified by Soxhlet extractions before reprecipitation to obtain the polymer material.

3. SAMPLE PREPARATION

As doctor-blading is impractical on the small quartz substrates used for the PL and WAXS measurements, drop-casting was used to prepare samples with as similar a film morphology to the final devices as possible. The drop-cast films were prepared of either neat polymer, by heating 10 mg mL^{-1} solutions, or of polymer:PCBM blends, by heating solutions containing 10 mg mL^{-1} of polymer and 20 mg mL^{-1} PCBM, in *o*-dichlorobenzene (*o*-DCB) to 100 °C for 12 h to ensure full dissolution of the polymer. The substrates used were z-cut quartz disks, cleaned by 10 min of Ar plasma etch, followed by three rounds of ultrasonication for 3 min each in isopropanol, acetone, and distilled water. A small volume of the polymer(:PCBM) solution (30 μL) was drop-cast directly onto the cleaned substrates, preheated to 100 °C on a hot plate, and left to dry and anneal for 5 min. For exciton diffusion length measurements, steady-state UV−vis absorption, and TIPL, spin-coated neat polymer films were prepared by heating a 20 mg mL^{-1} solution of polymer in *o*-DCB to 100 °C overnight. To prepare polymer films of different thickness, a 50 μL aliquot of the solution was removed 20 min before the film was spun and added to a second vial with pure *o*-DCB to make solutions of 1, 2, 5, and 10 mg mL^{-1} concentration. A small volume of each of these (25 μL) was dropped and spun on substrates for 5 s at 800 rpm and then 45 s at 2000 rpm, after which samples were annealed for 2 min at 100 °C. For steady-state UV−vis absorption and TIPL, quartz substrates were used which were cleaned in the same manner as those used for the drop-cast films. For exciton diffusion length measurements, substrates with a compact TiO_2 quencher layer were prepared by RF sputtering a layer of TiO_2 to 80 nm thickness, followed by an annealing step at 451 °C for 2 min under argon. This gave thin films with a surface roughness of approximately 2 nm as determined by AFM (see Supporting Information for details of sputtering conditions and AFM images). Before polymer deposition these substrates were cleaned with compressed air only. The film thickness of each of the polymer films on quartz was determined by use of a Dektak surface profiler. Solutions for temperature-dependent TCSPC and TIPL measurements were prepared by heating 10 mg mL^{-1} of polymer in *o*-DCB to 100 °C for 12 h and diluting down to 0.05 and 5 mg mL^{-1} without filtering. The solutions were heated to 90 °C for 30 min to ensure dissolution of the polymer before cooling to 10 °C to begin measurement.

Photovoltaic devices with the standard glass/ITO/PEDOT:PSS/polymer:PCBM/Ca/Al structure were prepared as follows: 1(1 + 1) ITO-coated glass substrates were cleaned by ultrasonication in acetone, isopropanol, and distilled water and layer (20 nm) of poly(3,4-ethylenedioxythiophene) poly(styrenesulfonate) (PEDOT/PSS, Clevios VP AI 4083, H.C. Starck) was deposited by spin-coating and then dried for 30 min at 130 °C in a nitrogen-filled glovebox.

A 40 mg mL^{-1} solution of either $PC_{60}BM$ (phenyl-C60-butyric acid methyl ester) or $PC_{70}BM$ (phenyl-C70-butyric acid methyl ester) in *o*-DCB and additional *o*-DCB (both by volume) were added to the polymer material to make a final solution of polymer:$PC_{60}BM$ (1:2) with total solid concentration of 30 mg mL^{-1} in *o*-DCB. This solution was heated to dissolve the solids and then held at 70 °C.

The active layer was deposited on top of the PEDOT:PSS-coated substrates by doctor blading on an Erichsen Coatmaster 509MC, using the following parameters: coating temperature, 70 °C; blade speed, 40 mm s^{-1}; screw gap, 0.03 mm; coating volume, 40 μL. The coated films were left to anneal for 2 min on a 70 °C hot plate. Top Ca/Al cathodes were deposited by thermal evaporation. Current density−voltage characteristics were taken with a Keithley 2420 digital source meter under standard 1 sun (AM1.5G) conditions, which were checked with a K5 filtered calibrated silicon reference diode.

4. RESULTS AND DISCUSSION

Figure 1 introduces the materials used in this study, which form a series of related low-bandgap polymers with active donor−

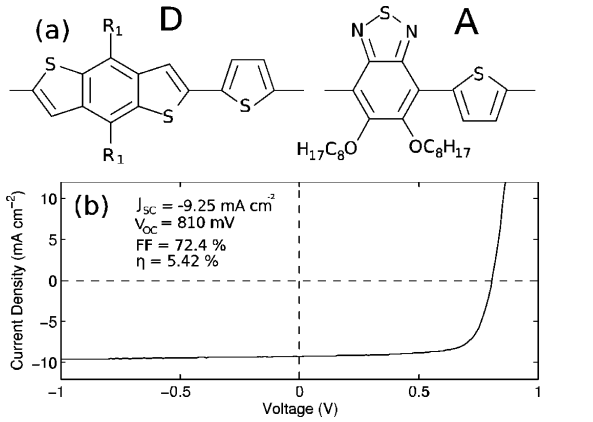

Figure 1. (a) Donor and acceptor moieties of which the materials used in this study are comprised. All polymers have the same benzothiadiazole acceptor group (R_2 = C_8H_{17}) and different alkyl side chains (R_1) on the benzodithiophene donor unit as described in Table 1. (b) Representative current density−voltage curve obtained from a device incorporating P5 blended with $PC_{60}BM$ as described in the Experimental Methods section. Each reported value is the mean value obtained from 10 individual photovoltaic cells on a single substrate.

acceptor units comprising 2,6-[benzodithiophene] acceptors and 2,5-thiophene-*co*-4,7-[5,6-dialkoxybenzothiadiazole]-*co*-2,5-thiophene (BDT) donors. The general structure of the donor and acceptor units is shown in Figure 1a, and Figure 1b shows a representative current density−voltage curve under solar simulator conditions for the best performing material (P5), for which a PCE value of 5.42% was observed. Details of the different alkyl side chains attached to the BDT unit, along with the number-average molecular weight, energy levels, and bandgap energy of each of the polymers, along with average measured PV parameters for polymer:$PC_{60}BM$ solar cell fabricated as described in the Experimental Methods section, are summarized in Table 1.

Small changes in alkyl chain length have a large effect (up to a factor of 2) on power conversion efficiency, but the values do

dx.doi.org/10.1021/jp504010x | J. Phys. Chem. C 2014, 118, 17351−17361

Table 1. Physical (Columns 2−4), Electrochemical (Columns 5−7), and Photovoltaic (Columns 8−11) Characteristics of the Five Polymers Used in This Study[a]

polymer	type	R_1 group	M_n [kDa]	HOMO [eV]	LUMO [eV]	E_g [eV]	V_{OC} [mV]	J_{SC} [mA cm^{-2}]	FF	PCE [%]
P1	LE	$C_{12}H_{25}$	21.6	−5.15	−3.33	1.82	667	5.33	55.7	1.98
P2	LE	C_8H_{17}	22.6	−5.30	−3.53	1.77	680	9.58	65.8	4.28
P3	LE	$C_{10}H_{21}$	15.3				697	5.34	33.1	1.23
P4	HE	$CH_2CH(C_2H_5)C_4H_9$	29.7	−5.33	−3.56	1.77	867	12.04	43.9	4.58
							(840)	(12.30)	(52.7)	(5.44)
P5	HE	$C_{12}H_{25}$	28.4	−5.34	−3.58	1.76	810	9.25	72.4	5.42
							(785)	(10.97)	(69.7)	(6.00)

[a]The polymer type refers to the two different approaches used in the chemical synthesis; the first approach yielding a system with LOW chain entropy (**P1** to **P3**) while the second resulted in systems with HIGH chain entropy (**P4** and **P5**). The number average molecular mass (M_n) along with the highest occupied molecular orbital (HOMO), lowest unoccupied molecular orbital (LUMO), and band gap (E_g) energies as determined from cyclic voltammetry measurements on thin film are also given. The photovoltaic properties are the open circuit voltage, V_{OC}; short circuit current, J_{SC}; fill factor, FF; and power conversion efficiency, PCE. Devices were prepared as described in the Sample Preparation section, with $PC_{60}BM$ as the electron acceptor. Values in parentheses were recorded when $PC_{70}BM$ was used instead. Devices were tested with 10−11 cells on a single substrate (cell area 4.5 mm^2 each), showing a typical standard deviation of ±0.25% to ±0.5% about the mean PCE values reported in the table.

not vary systematically with increasing alkyl chain length. Polymers **P1**−**P3** overall tend to exhibit lower photovoltaic efficiencies than polymers **P4** and **P5**, with the trend dominated by the higher J_{SC} of devices containing these materials. As we show below, such differences correlate with changes in the extent to which crystallite domains form in the films, and we therefore proceed to discuss evidence obtained for variations in film morphology.

Figure 2 shows steady-state absorption and emission spectra of the five polymers in dilute solution (a) and thin film (b). The

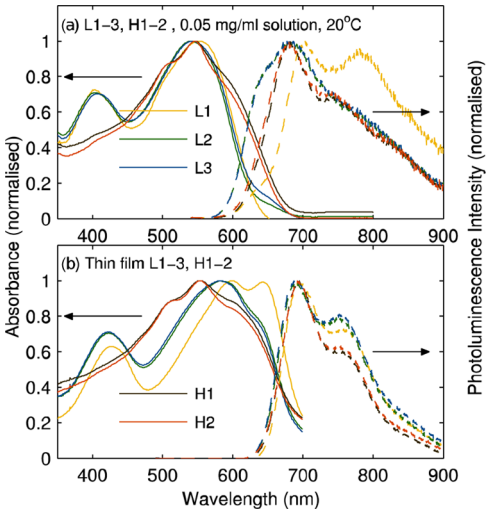

Figure 2. Steady-state absorbance and time-integrated photoluminescence spectra for all five polymers (a) in dilute (0.05 mg mL^{-1}) solution and (b) for thin (spin-cast) films at room temperature. For the PL spectra, samples were excited at 450 nm.

absorption onset shows a red-shift, broadening, and increase in vibronic structure on thin film formation, indicating increased interchain interactions,[38] with this effect being most pronounced in **P1** and least in **P4** and **P5**. Time-integrated PL of the solutions shows a strong red-shift in the emission spectrum of **P1** compared to that of the other polymers, indicating that for this polymer aggregation and interchain interactions are present even in dilute solutions. As with the absorption, a red-shift and increase in vibrational structure are observed in the PL following thin film formation, with the exception of polymer **P1**, in which the peak emission is unchanged between solution and thin film. This observation confirms that polymer **P1** forms extended aggregate domains comparable to those in thin film, even when in dilute solutions at room temperature.

In order to investigate the nature of aggregate domains in the polymer solid, wide-angle X-ray scattering measurements were performed on drop-cast polymer films. The deposition method used to prepare polymer thin films can affect the resulting morphology, with large differences observed between films prepared by spin-casting, in which solvent evaporates rapidly from the solution during spinning, and those prepared by doctor-blading, in which solvent evaporation occurs on a longer time scale.[39] In order to allow films to form with slower solvent evaporation, yet avoid difficulties associated with doctor-blading on small substrates, drop-casting was used to prepare the samples for WAXS and direct PL quenching measurements in polymer:fullerene blends. In Figure 3, the measured WAXS patterns show large differences between polymers **P1**−**P3** and **P4**−**P5**, with the former exhibiting a far higher degree of crystallinity while the latter two are almost entirely amorphous. Polymer **P1** is found to display the highest degree of crystallinity, in agreement with the above analysis of its UV−vis absorption and PL spectra. The three more crystalline materials exhibit a peak with a *d*-spacing of 2.11 nm in P1 and 1.78 nm in **P2** and **P3**, which has been assigned to the (100) interlamellar spacing in similar materials.[15,40] The absence of a discernible peak corresponding to a (010) plane π-stacking distance implies the more crystalline polymers forming π-stacked crystallites parallel to the substrate surface.[41] The higher intensity of the (100) peak in **P1** indicates a higher density of these crystalline domains in films of this material, with a lower degree of crystallization shown by **P2** and **P3** and mostly amorphous morphology for **P4** and **P5**. The inset to Figure 3a displays the effect of adding PCBM to the polymer with one example shown for each of the two types of polymer: the most crystalline **P1** and the mostly amorphous **P5**. The WAXS patterns of polymer:PCBM films show little difference to those of the corresponding neat polymer films; i.e., blending with PCMB seems to have little effect on the degree or size of polymer crystallites formed. The additional broad peak at 2θ = 20° (d = 3 Å) is attributed to the formation of PCBM crystallites in the film.[42,43]

The trends observed in WAXS patterns have a clear correspondence with surface topology of thin spin-cast films of the neat polymers. Figure 3b shows atomic force microscopy

dx.doi.org/10.1021/jp504010x | J. Phys. Chem. C 2014, 118, 17351−17361

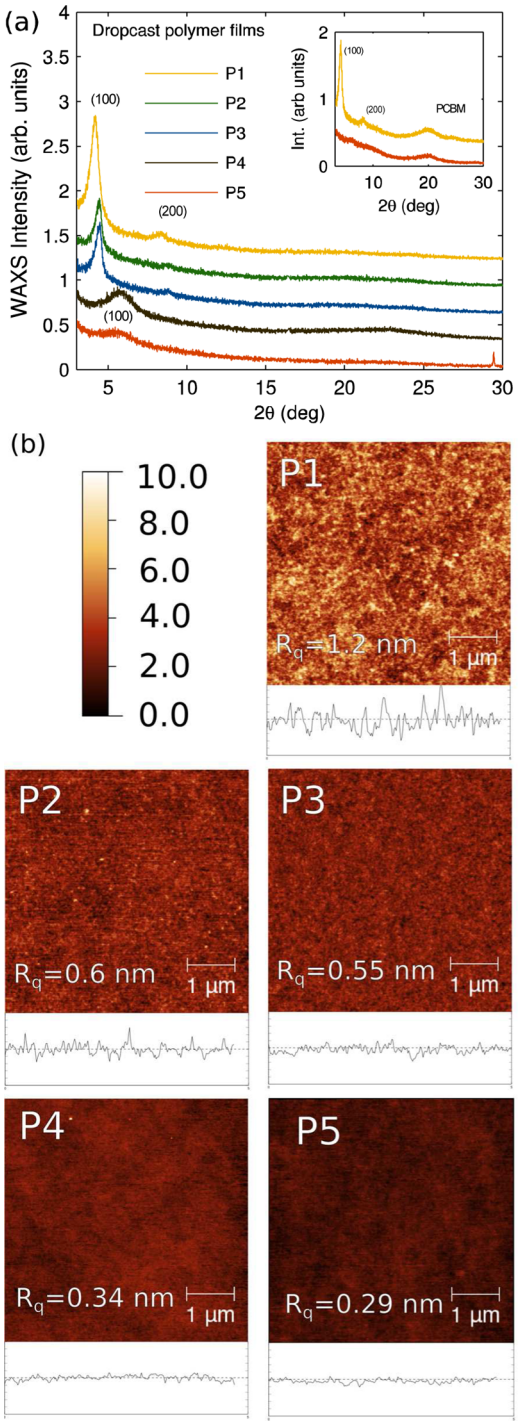

Figure 3. (a) Wide-angle X-ray diffraction spectra for drop-cast neat polymer films with curves offset from one another for clarity. The polymers **P1**, **P2**, and **P3** show a far higher degree of crystallinity than the relatively amorphous **P4** and **P5**, with **P1** being the most crystalline of all the materials studied. The strong peak at $2\theta = 4°$ corresponding to a repeat unit distance of approximately 2 nm is assigned to the distance between parallel polymer chains in the (100) plane,[64] with the small peak at $2\theta = 8°$ assigned to the second-order diffraction from the same plane. The inset shows WAXS patterns of P1:PCBM and P5:PCBM blend films prepared as described in the Experimental Methods section. (b) Topography images obtained by atomic force microscopy for neat films of all polymers. The black solid lines below each image show a typical height variation across the film from which the surface roughness R_q was determined for each film as shown on the respective AFM images.

images obtained for thin films of the five polymers, with a typical height variation contour shown below each image. The mean-square surface roughness of the most crystalline polymer **P1** was determined to be 1.2 nm, which is followed by a value of ~0.6 nm for the less crystalline **P2** and **P3**, and a roughness of 0.3 nm for the mostly amorphous polymers **P4** and **P5**. Enhanced surface roughness has in the past been associated with the presence of chain aggregates in the polymer film, as such domains may extend and protrude beyond the surface.[44] The clear correlation between crystallinity observed in WAXS patterns and surface roughness seen in AFM suggests that the formation of nanosized crystallites is also a prominent factor for these materials. We note that the polymer with the highest prevalence for crystallite domain formation (**P1**) shows poorest performance in photovoltaic devices, while the polymer that is most amorphous and displays least surface roughness (**P5**) has the highest photovoltaic power conversion efficiency in the series.

To unravel the reasons for the correlation between photovoltaic device performance and polymer film morphology, we proceed to examine the processes of exciton diffusion and interfacial dissociation in this material system. The presence of crystalline domains may affect the diffusion of excitons through the polymer, which may either be enhanced through the high order within a domain or impeded by the energetic barriers presented by additional interfaces at domain boundaries. The transfer of photogenerated excitation to the polymer−fullerene interface is a vital step in BHJ devices and radiative recombination of excitons before they reach an interface and dissociate can potentially be a large source of loss. In order to minimize this, the average distance over which excitons migrate before recombining should be equal to or greater than the polymer domain size.[45,46]

Various methods have been developed to determine the mean exciton diffusion length.[45,47,48] We used a time-resolved PL quenching method to investigate the influence of film crystallinity on the value of this parameter.[49,50] Thin films of varying thickness are excited, generating an excitation profile decaying exponentially from the excited film surface according to Beer's law (see Figure 4c). Polymer films are deposited on a flat TiO_2 layer, forming an interface at which electron transfer from the lowest unoccupied molecular orbital of the polymer to the conduction band of TiO_2 can occur. In sufficiently thin films, a large fraction of generated excitons can reach the polymer−TiO_2 interface, decreasing the observed PL lifetime as shown schematically in Figure 4c.[51] The PL emission dynamics for polymer films in the presence and absence of the electron acceptor are thus compared and modeled to obtain the exciton diffusion constant. A sputtered TiO_2 film thickness of 80 nm was used to minimize reflection of the 450 nm pump pulse used in the experiment and the initial distribution of excitons was assumed to follow a simple exponential depth profile according to the absorption at the excitation wavelength. A one-dimensional diffusion equation

$$\frac{\partial n(x,t)}{\partial t} = D\frac{\partial^2 n(x,t)}{\partial x^2} - \frac{n(x,t)}{\tau} \quad (1)$$

is used to model the distribution of excitons in the film, $n(x,t)$, at position x and time t after excitation, where D is the diffusion coefficient and τ is the photoluminescence lifetime determined by a monoexponential fit of the PL in the absence of any quencher material. If (i) the initial distribution of excitons,

dx.doi.org/10.1021/jp504010x | J. Phys. Chem. C 2014, 118, 17351−17361

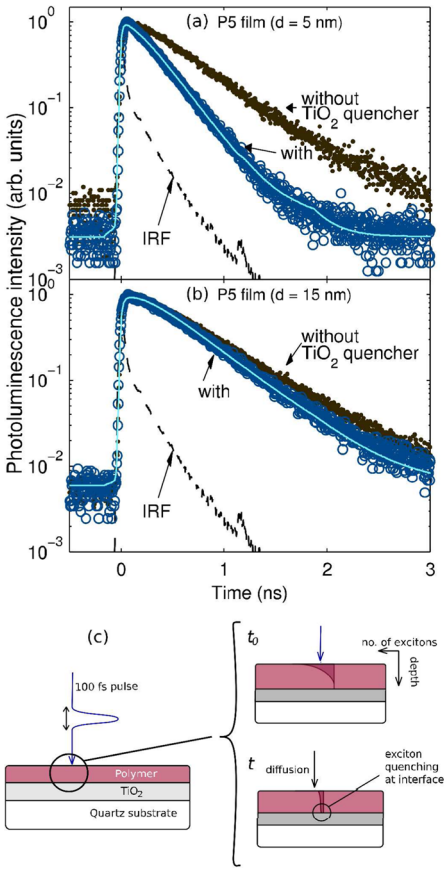

Figure 4. Photoluminscence decay transients measured for **P5** polymer films deposited on quartz substrates with (blue circles) and without (dark gray dots) an 80 nm thick coating of sputtered TiO_2. Data were taken with the TCSPC technique using a small-area silicon avalanche photodiode; the dashed line is the instrument response function (IRF) showing 35 ps fwhm. The solid light-blue line is a one-dimensional exciton diffusion model fit to the data by iterative reconvolution with the IRF, as described in the text and in the Supporting Information. The sole fitting parameter was D, the diffusion coefficient. Curves are shown for two different polymer film thicknesses: (a) 5 nm and (b) 15 nm. In each case, samples were excited from the front with pulses of 100 fs duration and 450 nm wavelength. The PL detection wavelength was 690 nm. The parameters extracted from fits to the curves are summarized in Table 2. Part c shows a schematic diagram of the diffusion length measurement. Following the initial excitation pulse, a distribution of excitons is created in the film. These excitons then diffuse until they recombine through intrinsic processes or reach the TiO_2:polymer interface where they are quenched.

$n(x,t_0)$, and film thickness, d, are known; (ii) any excitons that reach the TiO_2 interface are assumed to quench with unit efficiency; and (iii) any nonradiative (including surface quenching) effects are included in the overall decay lifetime τ, then D becomes the sole unknown and can be varied to fit the model to the measured decay curves.

Observation of the charge transfer step and free charge yields across organic semiconductor−TiO_x interfaces have been reported and range from relatively efficient (95% CT, 45% exciton to free charge conversion rate with terthiophene[52]) to highly inefficient (<1% free charge yield with P3PBT[53]). The values we observe therefore are a minimum possible diffusion length, as in systems with less than perfect charge transfer at the interface a longer diffusion length would be required to produce the same rate of PL quenching.

Figure 4 shows PL decay transients measured for thin films of polymer **P5** deposited on quartz substrates with and without the TiO_2 quencher for film thicknesses of approximately 6 and 15 nm. Corresponding measurements for polymers **P1** are given in the Supporting Information. The solid light-blue line in Figure 4 is the solution of the diffusion equation (eq 1), integrated over the film thickness and convoluted with the instrument response function (IRF). Here, solely the diffusion constant was varied in order to obtain best fits to the observed PL transients in the presence of the TiO_2 quencher. The procedure was carried out for both film thicknesses, which yielded good agreement, and values extracted for the diffusion coefficient and diffusion length, $L_D = (\tau D)^{1/2}$, are given in Table 2 together with the PL decay lifetime. The more crystalline **P1**

Table 2. Parameters Extracted from Fits to the PL Emission Transients Shown in Figure 4 and in the Supporting Information[a]

polymer	τ [ps]	D [10^{-3} cm^2 s^{-1}]	L_D [nm]
P1	350 ± 10	1.0 ± 0.3	7.4 ± 2.5
P5	450 ± 10	0.31 ± 0.15	4.0 ± 1.0

[a]Lifetimes determined from monoexponential fits to the PL transients in the absence of the quencher layer; exciton diffusion constant D extracted from modelling PL transients in the presence of a TiO_2 compact quencher layer; exciton diffusion length $L_D = (\tau D)^{1/2}$. The main source of the ∼30% error in the values for D is caused by inherent difficulties in determining the polymer film thickness.

exhibits an exciton diffusion coefficient that is approximately 3 times higher than that of the more amorphous **P5**. When taking into account the differing exciton lifetimes, the exciton diffusion length in **P1** is found to be about 85% higher than that in thin films of **P5**. We note that these discrepancies may in part be accounted for by the enhanced overlap between **P1** absorption and emission spectra (see Figure 2) which arise from the strong aggregation feature near the band edge of **P1**. According to Förster theory,[54,55] such spectral overlap will enhance exciton transfer between chromophores of the polymer, leading to faster exciton diffusion. We note that the observed trends in exciton diffusion lengths cannot automatically be assumed to also hold for charge carriers, as the mechanisms for charge transport may differ.

Differences in exciton diffusion lengths may have a strong impact on photovoltaic device efficiencies because they can, depending on the degree of phase segregation, affect the fraction of excitons reaching an interface in BHJ films. We therefore proceed to examine directly[56] the rates at which excitons are quenched in spin-coated BHJ films containing blends of polymer and PCBM in a 1:2 weight ratio. As a reference measurement, Figure 5a shows the measured PL transients for all five polymers in neat films (no PCBM). Interestingly, a clear difference between the mainly amorphous (**P4**, **P5**) and more crystalline (**P1**−**P3**) polymers can be seen, with the former displaying lifetimes of around 450 ps and the latter 350 ps. These differences do not depend on the wavelength at which the films are excited: the inset to Figure 5a shows the PL lifetime, τ, obtained from convoluted monoexponential fits to the PL transients obtained for thin films of polymers **P1** (crystalline) and **P4** (amorphous) following excitation at wavelengths between 370 and 650 nm.

dx.doi.org/10.1021/jp504010x | J. Phys. Chem. C 2014, 118, 17351−17361

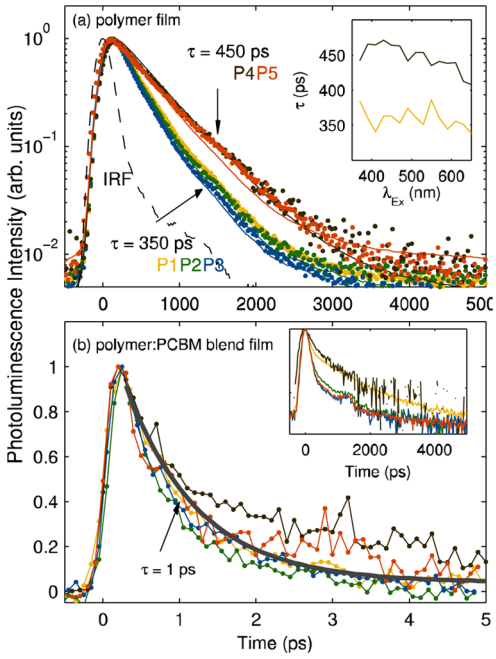

Figure 5. (a) Time-resolved photoluminescence transients on spin-cast films of neat polymer measured by TCPSC with excitation wavelength of 450 nm and detection wavelength set to 690 nm. The dashed line is the instrument response function (IRF) of the photomultiplier tube used for detection, showing 230 ps fwhm. The thin films of more crystalline (**P1**–**P3**) exhibit characteristic PL decay times of approximately 350 ps, whereas the amorphous polymers (**P4**, **P5**) show longer lifetimes of approximately 450 ps. The inset shows the PL lifetime extracted from response-convoluted monoexponential fits to the PL transients for **P4** and **P1** polymer films, as a function of the excitation wavelength. (b) Time-resolved PL transients of thin BHJ films of polymer:PCBM blends in a 1:2 ratio measured by PLUC with 350 fs time resolution (main figure) and TCSPC with 230 ps resolution (inset). The bold gray curve is a monoexponential decay with 1 ps lifetime included as a guide to the eye. As can be seen from the inset figure, there is some residual, longer-lived PL in the blend films with **P1** and **P4** at longer times, whereas decay curves for **P2**, **P3**, and **P5** all follow the instrument response.

The difference between the lifetimes measured for the two polymers is maintained across this range, and the lifetime appears to be largely independent of pump energy. For strongly aggregated polymer chains, a lengthening of the PL emission lifetimes would normally be expected, as the electronic coupling between molecules in H-aggregate conformation is known to reduce the oscillator strength of the coupled system.[57] However, in thin polymer films, excitons will rapidly diffuse to the most strongly aggregated regions because these have the lowest associated potential energy. As excitons reach such sites, their emissivity is gradually reduced, which appears as a rapid PL quenching that is mostly representative of the exciton diffusion rate to weakly emissive sites.

To assess the exciton quenching rate in polymer:PCBM BHJ films, PL transients were measured with high (350 fs) time resolution, as shown in Figure 5b. For all five polymers, the initial PL decay is predominantly very rapid, with lifetimes of the order of 1 ps. To examine the possible presence of residual slower decay components, lower resolution (230 ps), longer time PL decay curves were acquired using TCSPC, as shown in the inset of Figure 5b. There is a small amount of residual PL in blend films containing polymers **P1** and **P4** at longer times; however, the PL transients from the other films, **P2**, **P3** and **P5**, follow the instrument response, indicating that all PL is quenched within ∼200 ps after excitation. There is no clear correlation between the presence of such residuals and performance of the polymer in photovoltaics devices (see Table 1). This is not surprising given that for all polymers the majority (>90%) of excitons generated in BHJ films with PCBM reach an interface and are quenched within 5 ps after excitation. Such rapid quenching also means that the differences in exciton diffusion lengths observed for neat polymer films (Table 2) cannot have any significant influence on the efficiency of charge generation in the polymer blend with PCBM. Our measurements therefore suggest that these DA-copolymer:PCMB blends must exhibit a large volume fraction (>90%), for which the length scale of phase segregation falls significantly below the measured diffusion lengths (4–7.5 nm). The tendency of the polymer to form crystalline domains hence appears to have little effect on the initial exciton dissociation and must rather influence the remaining subsequent charge recombination and extraction steps.

Finally, we examine the extent to which the existence of aggregate domains in thin polymer films may be precipitated by agglomerations already present in solution prior to casting. There have been previous reports of polymer chain aggregates forming in solution which then persist into the cast film.[58] For such systems, the final film morphology may be particularly sensitive to solution temperature and casting conditions. In order to investigate such effects, we have measured the evolution of the emission spectra and transients of the five polymers in solution as the temperature is varied between 10 and 90 °C. For clarity and brevity, we present in Figures 6 and 7 only data for the polymers displaying the strongest (**P1**) and weakest (**P5**) crystallinity effects in thin films. Corresponding data for all other polymers are provided in the Supporting Information.

Figure 6 shows the time-resolved PL decay for **P1** and **P5**, recorded for emission wavelengths ranging from 600 to 850 nm, at low (10 °C) and high (90 °C, inset) solution temperature. The low-temperature (10 °C) dynamics are markedly different for the two polymers: **P1** displays a monoexponential PL decay at short wavelength, but exhibits a second, short-lived (τ_1 = 408 ps) contribution at longer wavelengths. The relative contributions of the two terms are extracted through monoexponential fitting and are plotted in Figure 6c as a function of emission wavelength. It appears that for **P1** in *o*-DCB solution two types of emitting species are present. Once the solution has been heated to 90 °C (inset to Figure 6a), however, only monoexponential decay dynamics are observed at all detection wavelengths. We therefore assign the short-lived component to the emission from chain aggregate clusters in solution, noting that their emission lifetime (408 ps) is only slightly longer than that for the thin film of the same polymer (340 ps); see Table 3. These observations imply that some of the crystalline domains found in **P1** films begin to form early during the casting process and are caused by an increased propensity of **P1** to aggregate in solution. All of the other polymers instead exhibit very different behavior, with an example given for **P5** in Figure 6b and for **P2**, **P3**, and **P4** in the Supporting Information. Monoexponential PL decays are observed at all solution temperatures with lifetimes τ_2 ranging between 1.45 and 1.75 ns (see Table 3). The observed additional slow PL rise at longer emission wavelengths is attributed to exciton relaxation to lower energy sites, possibly

dx.doi.org/10.1021/jp504010x | J. Phys. Chem. C 2014, 118, 17351–17361

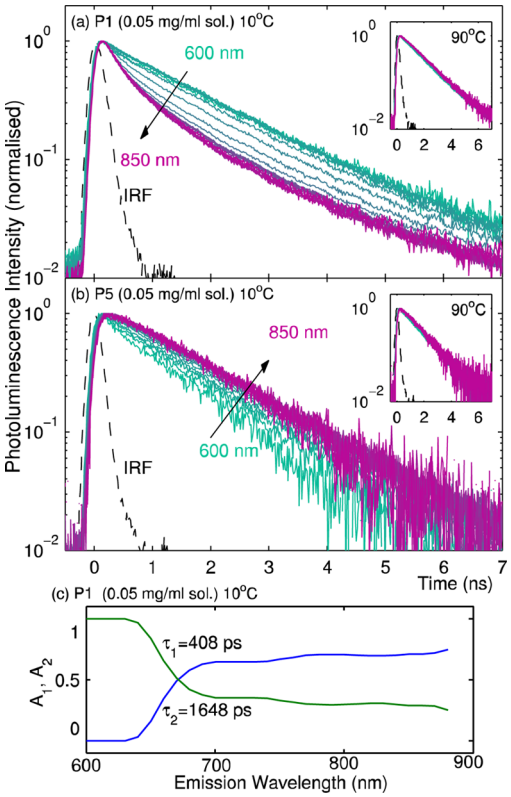

Figure 6. Photoluminescence decay transients for (a) **P1** and (b) **P5** solutions (0.05 mg mL^{-1}) in *o*-DCB at 10 °C (main figure) and 90 °C (inset). In each case, the excitation wavelength was held constant at 450 nm, and the time-resolved PL intensity measured at emission wavelengths ranging from 600 nm (green) to 850 nm (purple) in 10 nm steps. (c) Relative contribution to the overall PL arising from species emitting with lifetime τ_1 and those emitting with τ_2, shown for the case of **P1** at 10 °C. The values were extracted by fitting the sum of two monoexponentials with flexible amplitude fitting parameters A_1 and A_2 and two lifetimes as global fitting parameters.

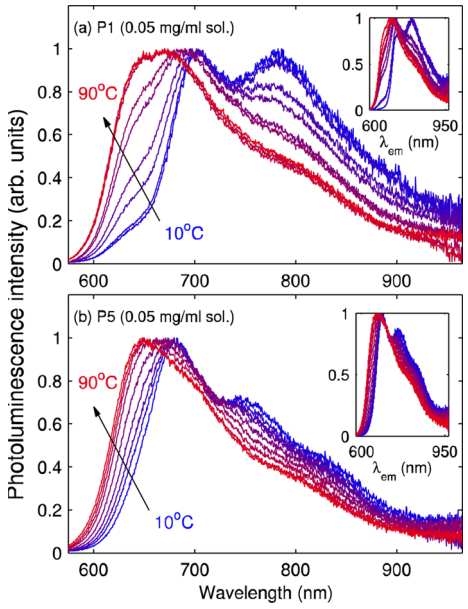

Figure 7. Time-integrated photoluminescence spectra for (a) **P1** and (b) **P5** polymers in 0.05 mg mL^{-1} solutions and 5 mg mL^{-1} (inset) of *o*-DCB at temperatures varying from 10 °C (blue) to 90 °C (red) in 10 ± 2 °C steps. The solutions were excited at a wavelength of 450 nm. The suppressed shoulder at ∼620 nm, which increases in intensity on increasing temperature (complete dissolution of the polymer), is indicative of H-aggregate formation of **P1** at low solution temperature. No such behavior is evident in solutions of the **P4** and **P5**, which form largely amorphous polymer films.

Table 3. PL Lifetimes Extracted from Monoexponential Fitting to PL Transients Recorded for Polymers P1−P5 in Solution (0.05 mg mL^{-1}) at 10 °C and for Drop-Cast Polymer Films[a]

	solution	thin film	
polymer	τ_1 [ps]	τ_2 [ps]	τ_{film} [ps]
P1	408	1648	340
P2		1757	321
P3		1765	299
P4		1474	502
P5		1456	443

[a]For solutions, **P1** is the only polymer to show contributions from two subspecies, exhibiting an additional short decay component τ_1 that is similar to τ_{film}.

within chain clusters that do not exhibit the strong interchain electronic coupling exhibited by polymer **P1**. At high temperatures (inset), all polymers are completely dissolved, and there is no migration to aggregate or lower energy sites in the ensemble.

To examine the effects upon polymer dissolution with increasing solvent temperature, we measured the time-integrated PL spectra for dilute (main figure) and high (inset) polymer concentrations at temperatures ranging from 10 to 90 °C (Figure 7 for **P1** and **P5** and Supporting Information for all other polymers). On increasing temperature, there is an overall broadening and loss in vibronic structure, along with a blue-shift of the peak emission. Such features may be related to a variety of effects, such as temperature-dependent changes in the dielectric constant, population of vibrational modes, and solvation effects. In addition, those materials forming more crystalline polymer films, in particular **P1** (Figure 7a) and to a lesser extent **P2** and **P3** (see Supporting Information), exhibit a decrease in the relative intensity of the high-energy shoulder (620 nm) with decreasing solution temperature. Such deviations from spectra that can be modeled as standard Franck−Condon vibrations progressions are indicative of H-aggregate formation.[59,60] These effects are absent in solutions of **P4** and **P5**, in agreement with the amorphous nature of thin films as evidenced by WAXS and AFM measurements.

Our examinations show that the way in which emission transients and spectra of polymer solutions evolve with temperature is an accurate predictor of the resulting morphology in the cast thin films. Thin films with high surface roughness and a large degree of crystallinity are cast for polymers such as **P1** that already in solution exhibit emission features and dynamics associated with chain aggregate formation. For polymers that form near-amorphous films (**P4** and **P5**) such features are entirely absent in solution. Polymers **P2** and **P3** are found to be intermediate cases, showing enhanced crystallinity and surface roughness in thin films and some non-Condon progressions in solution spectra. These findings suggest that for this type of polymer film morphology (and the related efficiency of photovoltaic devices) are

dx.doi.org/10.1021/jp504010x | J. Phys. Chem. C 2014, 118, 17351−17361

intimately linked with clustering in solution prior to casting. Attaining control over polymer solubility is therefore an important goal to achieve for this class of polymer.

5. SUMMARY

In summary, we have investigated the effects of thin-film morphology on factors affecting photovoltaic performance for a series of donor−acceptor copolymers comprising benzodithiophene and benzothiadiazole units. We find that the highest performing polymers in photovoltaic devices based on polymer:$PC_{60}BM$ blends are those showing the least degree of crystallinity in X-ray diffraction patterns and a corresponding lowest surface roughness in thin films. We find that the existence of such crystalline domains in thin polymer films correlates well with polymer chain aggregates being present already in solution prior to casting of the film. Polymer solubility and casting conditions therefore appear to be crucial factors for the development of photovoltaic devices with enhanced efficiencies. To examine why the presence of crystallite domains appears to hamper photovoltaic performance, we measured exciton diffusion lengths by modeling the observed migration of excitons through a thin polymer film deposited on a PL quencher layer of TiO_2. We find that diffusion lengths in these materials are substantial (4−7.5 nm) and show some variation between different polymer materials. However, ultrafast (1 ps) quenching of the PL from polymer:PCBM blends indicates that the vast majority of excitons created in polymer domains is not prevented from reaching an interface with PCBM, and hence exciton diffusion does not represent a limiting factor. These observations suggest that the subsequent charge extraction and lifetimes must be adversely affected by the presence of crystalline domains. We note that although extended crystalline polymer networks promote high hole mobilities within such domains,[61,62] the interfacial regions between well-ordered and amorphous polymer domains may act as energy barriers to charge transfer, forming sites at which charge trapping and recombination may occur with higher frequency.[34] The effect of the total polymer film crystallinity on the overall charge mobility is therefore a trade-off between these two factors. In materials such as P3HT[15] and some similar low-bandgap polymers[63] in which the polymer forms extended crystalline networks, the effect of in-domain charge mobility improvement will dominate and an increase in total crystallinity will enhance device efficiency. However, for polymers prone to the formation of small crystallites, an increase in total film crystallinity will increase the concentration of domain boundaries and hence lead to a reduction in overall charge mobility. The donor−acceptor polymers studied here clearly fall into the latter category, and as a result, polymers in this series appear to be the better suited for use in photovoltaic devices the more amorphous they are in the solid films. Our results have important implications for the design of such donor−acceptor copolymers for photovoltaics, suggesting that synthesis efforts may focus on creating polymers which exhibit sufficiently high inherent entropy.

■ ASSOCIATED CONTENT

Supporting Information

Deposition method and characterization of TiO_2 quencher films, modeling of exciton diffusion, time-resolved PL transients of films of **P1** with and without quencher layer, time-resolved PL transients of polymers **P1**−**P5** in solution, temperature-dependent steady-state PL emission for polymers **P1**−**P5** in solution, physical characteristics of polymers **P1**−**P5**, and separation of optical parameters from measured J_{SC}. This material is available free of charge via the Internet at http://pubs.acs.org.

■ AUTHOR INFORMATION

Corresponding Author

*E-mail: l.herz@physics.ox.ac.uk (L.M.H.).

Notes

The authors declare no competing financial interest.

■ ACKNOWLEDGMENTS

C.M. thanks the Engineering and Physical Sciences Research Council and Merck Chemicals for financial support through a CASE studentship. The Australian Research Council and Australian National Fabrication Facility are acknowledged for financial and facility support, respectively.

■ ABBREVIATIONS

TIPL, time-integrated photoluminescence; TCSPC, time-correlated single photon counting; PLUC, photoluminescence up-conversion; IRF, instrument response function; WAXS, wide-angle X-ray scattering; PCBM, phenyl-C61-butyric acid methyl ester; PEDOT:PSS, poly(3,4-ethylenedioxythiophene)−poly(styrenesulfonate); *o*-DCB, *o*-dichlorobenzene; ITO, indium tin oxide; P3HT, poly(3-hexylthiophene); P3PBT, poly[3-(potassium 4-butanoate)thiophene-2,5-diyl].

■ REFERENCES

(1) Kopola, P.; Aernouts, T.; Sliz, R.; Guillerez, S.; Ylikunnari, M.; Cheyns, D.; Välimäki, M.; Tuomikoski, M.; Hast, J.; Jabbour, G.; et al. Gravure Printed Flexible Organic Photovoltaic Modules. *Sol. Energy Mater. Sol. Cells* **2011**, *95*, 1344−1347.

(2) Hoth, C. N.; Choulis, S. A.; Schilinsky, P.; Brabec, C. J. High Photovoltaic Performance of Inkjet Printed Polymer:Fullerene Blends. *Adv. Mater.* **2007**, *19*, 3973−3978.

(3) Tang, C. W. Two-Layer Organic Photovoltaic Cell. *Appl. Phys. Lett.* **1986**, *48*, 183−185.

(4) Sariciftci, N. S.; Braun, D.; Zhang, C.; Srdanov, V. I.; Heeger, A. J.; Stucky, G.; Wudl, F. Semiconducting Polymer-Buckminsterfullerene Heterojunctions: Diodes, Photodiodes, and Photovoltaic Cells. *Appl. Phys. Lett.* **1993**, *62*, 585−587.

(5) Yu, G.; Gao, J.; Hummelen, J. C.; Wudl, F.; Heeger, A. J. Polymer Photovoltaic Cells: Enhanced Efficiencies via a Network of Internal Donor-Acceptor Heterojunctions. *Science* **1995**, *270*, 1789−1791.

(6) He, Z.; Zhong, C.; Su, S.; Xu, M.; Wu, H.; Cao, Y. Enhanced Power-Conversion Efficiency in Polymer Solar Cells Using an Inverted Device Structure. *Nat. Photonics* **2012**, *6*, 593−597.

(7) Zhou, H.; Yang, L.; Stoneking, S.; You, W. A Weak Donor−Strong Acceptor Strategy to Design Ideal Polymers for Organic Solar Cells. *ACS Appl. Mater. Interfaces* **2010**, *2*, 1377−1383.

(8) Guo, J.; Ohkita, H.; Benten, H.; Ito, S. Charge Generation and Recombination Dynamics in Poly(3-hexylthiophene)/Fullerene Blend Films with Different Regioregularities and Morphologies. *J. Am. Chem. Soc.* **2010**, *132*, 6154−6164.

(9) Coakley, K. M.; Srinivasan, B. S.; Ziebarth, J. M.; Goh, C.; Liu, Y.; McGehee, M. D. Enhanced Hole Mobility in Regioregular Polythiophene Infiltrated in Straight Nanopores. *Adv. Funct. Mater.* **2005**, *15*, 1927−1932.

(10) Schilinsky, P.; Asawapirom, U.; Scherf, U.; Biele, M.; Brabec, C. J. Influence of the Molecular Weight of Poly(3-hexylthiophene) on the Performance of Bulk Heterojunction Solar Cells. *Chem. Mater.* **2005**, *17*, 2175−2180.

(11) Szarko, J. M.; Guo, J.; Liang, Y.; Lee, B.; Rolczynski, B. S.; Strzalka, J.; Xu, T.; Loser, S.; Marks, T. J.; Yu, L.; et al. When Function

Follows Form: Effects of Donor Copolymer Side Chains on Film Morphology and BHJ Solar Cell Performance. *Adv. Mater.* **2010**, *22*, 5468−5472.
(12) Hiorns, R. C.; de Bettignies, R.; Leroy, J.; Bailly, S.; Firon, M.; Sentein, C.; Khoukh, A.; Preud'homme, H.; Dagron-Lartigau, C. High Molecular Weights, Polydispersities, and Annealing Temperatures in the Optimization of Bulk-Heterojunction Photovoltaic Cells Based on Poly(3-hexylthiophene) or Poly(3-butylthiophene). *Adv. Funct. Mater.* **2006**, *16*, 2263−2273.
(13) Lee, S.-H.; Kim, D.-H.; Kim, J.-H.; Lee, G.-S.; Park, J.-G. Effect of Metal-Reflection and Surface-Roughness Properties on Power-Conversion Efficiency for Polymer Photovoltaic Cells. *J. Phys. Chem. C* **2009**, *113*, 21915−21920.
(14) Lee, S.-H.; Kim, J.-H.; Shim, T.-H.; Park, J.-G. Effect of Interface Thickness on Power Conversion Efficiency of Polymer Photovoltaic Cells. *Electron. Mater. Lett.* **2009**, *5*, 47−50.
(15) Kim, Y.; Cook, S.; Tuladhar, S. M.; Choulis, S. a.; Nelson, J.; Durrant, J. R.; Bradley, D. D. C.; Giles, M.; McCulloch, I.; Ha, C.-S.; et al. A Strong Regioregularity Effect in Self-Organizing Conjugated Polymer Films and High-Efficiency Polythiophene:Fullerene Solar Cells. *Nat. Mater.* **2006**, *5*, 197−203.
(16) Li, G.; Yao, Y.; Yang, H.; Shrotriya, V.; Yang, G.; Yang, Y. "Solvent Annealing" Effect in Polymer Solar Cells Based on Poly(3-hexylthiophene) and Methanofullerenes. *Adv. Funct. Mater.* **2007**, *17*, 1636−1644.
(17) Savenije, T. J.; Kroeze, J. E.; Yang, X.; Loos, J. The Formation of Crystalline P3HT Fibrils upon Annealing of a PCBM: P3HT Bulk Heterojunction. *Thin Solid Films* **2006**, *511*, 2−6.
(18) Woo, C. H.; Thompson, B. C.; Kim, B. J.; Toney, M. F.; Fréchet, J. M. J. The Influence of Poly(3-hexylthiophene) Regioregularity on Fullerene-Composite Solar Cell Performance. *J. Am. Chem. Soc.* **2008**, *130*, 16324−16329.
(19) Schaffer, C. J.; Palumbiny, C. M.; Niedermeier, M.; Jendrzejewski, C.; Santoro, G.; Roth, S. V.; Müller-Buschbaum, P. A Direct Evidence of Morphological Degradation on a Nanometer Scale in Polymer Solar Cells. *Adv. Mater.* **2013**, *25*, 6760−6764.
(20) Ebadian, S.; Gholamkhass, B.; Shambayati, S.; Holdcroft, S.; Servati, P. Effects of Annealing and Degradation on Regioregular Polythiophene-Based Bulk Heterojunction Organic Photovoltaic Devices. *Sol. Energy Mater. Sol. Cells* **2010**, *94*, 2258−2264.
(21) Zhang, Y.; Yip, H.-L.; Acton, O.; Hau, S. K.; Huang, F.; Jen, A. K.-Y. A Simple and Effective Way of Achieving Highly Efficient and Thermally Stable Bulk-Heterojunction Polymer Solar Cells Using Amorphous Fullerene Derivatives as Electron Acceptor. *Chem. Mater.* **2009**, *21*, 2598−2600.
(22) Liang, Y.; Xu, Z.; Xia, J.; Tsai, S.-T.; Wu, Y.; Li, G.; Ray, C.; Yu, L. For the Bright Future - Bulk Heterojunction Polymer Solar Cells with Power Conversion Efficiency of 7.4%. *Adv. Mater.* **2010**, *22*, E135−E138.
(23) Zhong, H.; Li, Z.; Deledalle, F.; Fregoso, E. C.; Shahid, M.; Fei, Z.; Nielsen, C. B.; Yaacobi-Gross, N.; Rossbauer, S.; Anthopoulos, T. D. Fused Dithienogermolodithiophene Low Band Gap Polymers for High-Performance Organic Solar Cells without Processing Additives. *J. Am. Chem. Soc.* **2013**, *135*, 2040−2043.
(24) Osaka, I.; Kakara, T.; Takemura, N.; Koganezawa, T.; Takimiya, K. Naphthodithiophene-naphthobisthiadiazole Copolymers for Solar Cells: Alkylation Drives the Polymer Backbone Flat and Promotes Efficiency. *J. Am. Chem. Soc.* **2013**, *135*, 8834−8837.
(25) Dhanabalan, A.; van Duren, J. K. J.; van Hal, P. A.; van Dongen, J. L. J.; Janssen, R. A. J. Synthesis and Characterization of a Low Bandgap Conjugated Polymer for Bulk Heterojunction Photovoltaic Cells. *Adv. Funct. Mater.* **2001**, *11*, 255−262.
(26) van Duren, J. K. J.; Dhanabalan, A.; van Hal, P. A.; Janssen, R. A. J. Low-bandgap Polymer Photovoltaic Cells. *Synth. Met.* **2001**, *121*, 1587−1588.
(27) Brabec, C. J.; Winder, C.; Sariciftci, N. S.; Hummelen, J. C.; Dhanabalan, A.; van Hal, P. A.; Janssen, R. A. J. A Low-Bandgap Semiconducting Polymer for Photovoltaic Devices and Infrared Emitting Diodes. *Adv. Funct. Mater.* **2002**, *12*, 709−712.
(28) Bundgaard, E.; Krebs, F. C. Low Band Gap Polymers for Organic Photovoltaics. *Sol. Energy Mater. Sol. Cells* **2007**, *91*, 954−985.
(29) Zhang, Q. T.; Tour, J. M. Low Optical Bandgap Polythiophenes by an Alternating Donor/Acceptor Repeat Unit Strategy. *J. Am. Chem. Soc.* **1997**, *119*, 5065−5066.
(30) Brocks, G.; Tol, A. Small Band Gap Semiconducting Polymers Made from Dye Molecules: Polysquaraines. *J. Phys. Chem.* **1996**, *100*, 1838−1846.
(31) Beiley, Z. M.; Hoke, E. T.; Noriega, R.; Dacuña, J.; Burkhard, G. F.; Bartelt, J. a.; Salleo, A.; Toney, M. F.; McGehee, M. D. Morphology-Dependent Trap Formation in High Performance Polymer Bulk Heterojunction Solar Cells. *Adv. Energy Mater.* **2011**, *1*, 954−962.
(32) Wang, E.; Bergqvist, J.; Vandewal, K.; Ma, Z.; Hou, L.; Lundin, A.; Himmelberger, S.; Salleo, A.; Müller, C.; Inganäs, O.; et al. Conformational Disorder Enhances Solubility and Photovoltaic Performance of a Thiophene-Quinoxaline Copolymer. *Adv. Energy Mater.* **2013**, *3*, 806−814.
(33) Tumbleston, J. R.; Stuart, A. C.; Gann, E.; You, W.; Ade, H. Fluorinated Polymer Yields High Organic Solar Cell Performance for a Wide Range of Morphologies. *Adv. Funct. Mater.* **2013**, *23*, 3463−3470.
(34) Spoltore, D.; Oosterbaan, W. D.; Khelifi, S.; Clifford, J. N.; Viterisi, A.; Palomares, E.; Burgelman, M.; Lutsen, L.; Vanderzande, D.; Manca, J. Effect of Polymer Crystallinity in P3HT:PCBM Solar Cells on Band Gap Trap States and Apparent Recombination Order. *Adv. Energy Mater.* **2013**, *3*, 466−471.
(35) Pan, H.; Li, Y.; Wu, Y.; Liu, P.; Ong, B. S.; Zhu, S.; Xu, G. Synthesis and Thin-Film Transistor Performance of Poly(4,8-didodecylbenzo[1,2-b:4,5-b′]dithiophene). *Chem. Mater.* **2006**, *18*, 3237−3241.
(36) Bouffard, J.; Swager, T. M. Fluorescent Conjugated Polymers That Incorporate Substituted 2,1,3-Benzooxadiazole and 2,1,3-Benzothiadiazole Units. *Macromolecules* **2008**, *41*, 5559−5562.
(37) Tierney, S.; Heeney, M.; McCulloch, I. Microwave-Assisted Synthesis of Polythiophenes via the Stille Coupling. *Synth. Met.* **2005**, *148*, 195−198.
(38) Barnes, M. D.; Baghar, M. Optical Probes of Chain Packing Structure and Exciton Dynamics in Polythiophene Films, Composites, and Nanostructures. *J. Polym. Sci., Part B: Polym. Phys.* **2012**, 1121−1129.
(39) Mens, R.; Bertho, S.; Chambon, S.; D'Haen, J.; Lutsen, L.; Manca, J.; Gelan, J.; Vanderzande, D.; Adriaensens, P. Solid-State NMR as a Tool To Describe and Quantify the Morphology of Photoactive Layers Used in Plastic Solar Cells. *J. Polym. Sci., Part A: Polym. Chem.* **2011**, *49*, 1699−1707.
(40) Han, H.; Lee, H.; Nam, S.; Jeong, J.; Lee, I.; Kim, H.; Ha, C.-S.; Kim, Y. Poly(3-hexylthiophene-co-benzothiadiazole) (THBT) as an Electron-Accepting Polymer for Normal and Inverted Type All-Polymer Solar Cells. *Polym. Chem.* **2013**, *4*, 2053−2061.
(41) Erb, T.; Zhokhavets, U.; Gobsch, G.; Raleva, S.; Stühn, B.; Schilinsky, P.; Waldauf, C.; Brabec, C. J. Correlation Between Structural and Optical Properties of Composite Polymer/Fullerene Films for Organic Solar Cells. *Adv. Funct. Mater.* **2005**, *15*, 1193−1196.
(42) Mens, R.; Chambon, S.; Bertho, S.; Reggers, G.; Ruttens, B.; D'Haen, J.; Manca, J.; Carleer, R.; Vanderzande, D.; Adriaensens, P. Description of the Nanostructured Morphology of [6,6]-Phenyl-C61-butyric Acid Methyl Ester (PCBM) by XRD, DSC and Solid-State NMR. *Magn. Reson. Chem.* **2011**, *49*, 242−247.
(43) Colle, R.; Grosso, G.; Ronzani, A.; Gazzano, M.; Palermo, V. Anisotropic Molecular Packing of Soluble C60 Fullerenes in Hexagonal Nanocrystals Obtained by Solvent Vapor Annealing. *Carbon* **2012**, *50*, 1332−1337.
(44) Blatchford, J. W.; Gustafson, T. L.; Epstein, A. J.; Vanden Bout, D. A.; Kerimo, J.; Higgins, D. A.; Barbara, P. F.; Fu, D. K.; Swager, T. M.; MacDiarmid, A. G. Spatially and Temporally Resolved Emission from Aggregates in Conjugated Polymers. *Phys. Rev. B* **1996**, *54*, R3683−R3686.

(45) Mikhnenko, O. V.; Azimi, H.; Scharber, M.; Morana, M.; Blom, P. W. M.; Loi, M. A. Exciton Diffusion Length in Narrow Bandgap Polymers. *Energy Environ. Sci.* **2012**, *5*, 6960−6965.
(46) Scully, S. R.; Armstrong, P. B.; Edder, C.; Fréchet, J. M. J.; Mcgehee, M. D. Long-Range Resonant Energy Transfer for Enhanced Exciton Harvesting for Organic Solar Cells. *Adv. Mater.* **2007**, *19*, 2961−2966.
(47) Lin, J. D. A.; Mikhnenko, O. V.; Chen, J.; Masri, Z.; Ruseckas, A.; Mikhailovsky, A.; Raab, R. P.; Liu, J.; Blom, P. W. M.; Loi, M. A.; et al. Systematic Study of Exciton Diffusion Length in Organic Semiconductors by Six Experimental Methods. *Mater. Horiz.* **2014**, *1*, 280−285.
(48) Haugeneder, A.; Neges, M.; Kallinger, C.; Spirkl, W.; Lemmer, U.; Feldmann, J.; Scherf, U.; Harth, E.; Gügel, A.; Müllen, K. Exciton Diffusion and Dissociation in Conjugated Polymer Fullerene Blends and Heterostructures. *Phys. Rev. B* **1999**, *59*, 15346−15351.
(49) Markov, D. E.; Tanase, C.; Blom, P. W. M.; Wildeman, J. Simultaneous Enhancement of Charge Transport and Exciton Diffusion in Poly(p-phenylene vinylene) Derivatives. *Phys. Rev. B* **2005**, *72*, 045217.
(50) Shaw, P. E.; Ruseckas, A.; Samuel, I. D. W. Exciton Diffusion Measurements in Poly(3-hexylthiophene). *Adv. Mater.* **2008**, *20*, 3516−3520.
(51) Förster, T. Energiewanderung und Fluoreszenz. *Naturwissenschaften* **1946**, *33*, 166−175.
(52) Helbig, M.; Ruseckas, A.; Grage, M. M.-L.; Birckner, E.; Rentsch, S.; Sundström, V. Resolving the Radical Cation Formation from the Lowest-Excited Singlet (S1) State of Terthiophene in a TiO_2−SiO_2 Hybrid Polymer Matrix. *Chem. Phys. Lett.* **1999**, *302*, 587−594.
(53) Segal-Peretz, T.; Leman, O.; Nardes, A. M.; Frey, G. L. On the Origin of Charge Generation in Hybrid TiO_x/Conjugated Polymer Photovoltaic Devices. *J. Phys. Chem. C* **2012**, *116*, 2024−2032.
(54) Förster, T. Transfer Mechanisms of Electronic Excitation. *Discuss. Faraday Soc.* **1959**, *27*, 7−17.
(55) Guilbert, A. A. Y.; Reynolds, L. X.; Bruno, A.; MacLachlan, A.; King, S. P.; Faist, M. A.; Pires, E.; Macdonald, J. E.; Stingelin, N.; Haque, S. A.; et al. Effect of Multiple Adduct Fullerenes on Microstructure and Phase Behavior of P3HT:Fullerene Blend Films for Organic Solar Cells. *ACS Nano* **2012**, *6*, 3868−3875.
(56) Kasha, M. Energy Transfer Mechanisms and the Molecular Exciton Model for Molecular Aggregates. *Radiat. Res.* **1963**, *20*, 55−70.
(57) Nguyen, T.-Q.; Doan, V.; Schwartz, B. J. Conjugated Polymer Aggregates in Solution: Control of Interchain Interactions. *J. Chem. Phys.* **1999**, *110*, 4068−4078.
(58) Yamagata, H.; Spano, F. C. Interplay Between Intrachain and Interchain Interactions in Semiconducting Polymer Assemblies: The HJ-Aggregate Model. *J. Chem. Phys.* **2012**, *136*, 184901.
(59) Parkinson, P.; Müller, C.; Stingelin, N.; Johnston, M. B.; Herz, L. M. Role of Ultrafast Torsional Relaxation in the Emission from Polythiophene Aggregates. *J. Phys. Chem. Lett.* **2010**, *1*, 2788−2792.
(60) Chang, J.-F.; Sun, B.; Breiby, D. W.; Nielsen, M. M.; Sölling, T. I.; Giles, M.; McCulloch, I.; Sirringhaus, H. Enhanced Mobility of Poly(3-hexylthiophene) Transistors by Spin-Coating from High-Boiling-Point Solvents. *Chem. Mater.* **2004**, *16*, 4772−4776.
(61) Bao, Z.; Dodabalapur, A.; Lovinger, A. J. Soluble and Processable Regioregular Poly(3-hexylthiophene) for Thin Film Field-Effect Transistor Applications with High Mobility. *Appl. Phys. Lett.* **1996**, *69*, 4108−4110.
(62) Zhang, M.; Gu, Y.; Guo, X.; Liu, F.; Zhang, S.; Huo, L.; Russell, T. P.; Hou, J. Efficient Polymer Solar Cells Based on Benzothiadiazole and Alkylphenyl Substituted Benzodithiophene with a Power Conversion Efficiency over 8%. *Adv. Mater.* **2013**, *25*, 4944−4949.
(63) Markov, D. E.; Amsterdam, E.; Blom, P. W. M.; Sieval, A. B.; Hummelen, J. C. Accurate Measurement of the Exciton Diffusion Length in a Conjugated Polymer Using a Heterostructure with a Side-Chain Cross-Linked Fullerene Layer. *J. Phys. Chem. A* **2005**, *109*, 5266−5274.
(64) Chiu, M.-Y.; Jeng, U.-S.; Su, M.-S.; Wei, K.-H. Morphologies of Self-Organizing Regioregular Conjugated Polymer/Fullerene Aggregates in Thin Film Solar Cells. *Macromolecules* **2010**, *43*, 428−432.